On the Electron Density Topology and Electrostatic Properties of Nitroanilines. A Theoretical Investigation on *m*-Nitroaniline and 2-Methyl-5-nitroaniline Crystals

Adolfo C. Fantoni,* C. Gustavo Pozzi, and Graciela Punte

IFLP (CCT-La Plata), Departamento de Física, Facultad de Ciencias Exactas, UNLP CC 67, 1900 La Plata, Argentina

Received: May 8, 2009; Revised Manuscript Received: June 30, 2009

On the basis of the AIM theory, intermolecular interactions have been characterized in the B3LYP/6-31G** periodic electron density of the title compounds. Although the set of bond paths identified in each system is not fully equivalent to its experimental counterpart, agreement is reasonable with regard to the nature and relative importance of the intermolecular interactions at play. Within the AIM partition scheme, the molecular dipole moment of the in-crystal molecule was determined for the title compounds and the two closely related crystals of 2-methyl-4-nitroaniline and *p*-nitroaniline. Using a method that relies only on molecular calculations and a mean electric field approximation, it was possible to reproduce within 6% the values of the molecular dipole moment modulus obtained directly from the periodic electron densities. This result reveals that, for this kind of molecular crystal, enhancement of the dipole moment in going from the isolated molecule to the in-crystal one is an almost exclusively inductive effect.

Introduction

The nonlinear optical (NLO) properties of some organic materials have received renewed attention in the past years[1−4] due to their potential technological applications, either on their own or forming hybrid materials.[5,6] Nitroanilines are typical examples of this kind of compound, since the coexistence of an electron-rich and an electron-deficient substituent, connected through a conjugated π electronic system, makes their molecular second-order hyperpolarizability and second-harmonic generation efficiency particularly high.

However, if the crystal structure is centrosymmetric, NLO properties are lost in the solid. Packing then plays a crucial role from the viewpoint of some technological applications, and it would be desirable to have tools to guide assembling toward a particular polymorph. Comparative analyses of the electron density topology and electrostatic properties of closely related compounds can give hints on the relative importance of the different intermolecular interactions at play and the way they combine to lead to a particular structural pattern. Electron densities in the solid state can be determined either from theoretical calculations or from high resolution X-ray diffraction data. Both approaches have pros and cons. In the latter, a multipole model[7] is fitted against structure factors obtained from measured intensities, and because of that the resulting electron density is usually called experimental charge density. For molecular systems like nitroanilines, however, the number of parameters that could in principle be fitted is large, and they are usually highly correlated. Results can then hardly be independent of the particular criterion adopted in each case, this being in turn conditioned by the quality of the available data set. In a recent review,[8] where the results of several experimental charge density studies are critically analyzed, it is shown that molecular dipole moment values differing as much as 100% can result for the same compound.

With regard to theoretical electron densities, to the best of our knowledge, HF/DFT hybrid methods are at present the best available choice for electronic structure calculations in molecular periodic systems, and, as it is well-known, dispersive interactions are poorly modeled. But, while this deficiency makes meaningless the calculation of lattice energies, topological and electrostatic properties can be expected to be much less affected, mainly in relative terms. In the same review mentioned above,[8] where the apparently systematic differences between experimental charge density results and theoretical calculations with regard to molecular dipole moment enhancement are discussed, the lack of periodic theoretical calculations exploring the separate roles of the crystal field and hydrogen bonding is pointed out.

With all this in mind, we decided to study some electrostatic and topological properties of the theoretically determined electron densities of *m*-nitroaniline (mNA) and 2-methyl-5-nitroaniline (2M5NA) crystals. Some calculations were also performed for the closely related 2-methyl-4-nitroaniline (2M4NA) and *p*-nitroaniline (pNA) crystals. A bit of an effort was also devoted to ascertain whether noninductive effects play a significant role with regard to molecular dipole moment enhancement in going from the isolated molecule to the crystal. The obtained results and conclusions are presented in what follows.

Calculations

Periodic calculations (PC) were performed with the CRYSTAL98 program[9] using the B3LYP hybrid method with the 6-31G** basis set. Shrinking factors equal to 4 were used for both the Pack−Monkhorst and Gilat nets. Default criteria were used with regard to accuracy and SCF convergence. For each compound, a periodic electron density was also obtained as a superposition of molecular densities, with the molecules arranged as in the respective crystal (MOLSPLIT density).

The AIM[10] topological analysis of the resulting electron densities was performed with the TOPOND code,[11] using a combination of the available methods. The same code was used

* To whom correspondence should be addressed. Tel.: +54 2214230122. Fax: +54 2214236335. E-mail address: fantoni@fisica.unlp.edu.ar.

10.1021/jp904318q CCC: $40.75
Published on Web 08/04/2009

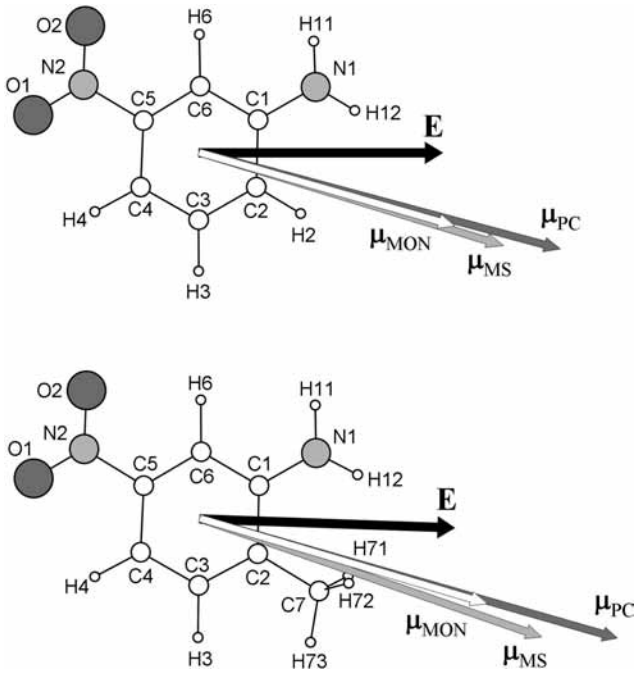

Figure 1. Atom labeling for mNA (above) and 2M5NA (below). Average electric field (**E**) and molecular dipole moments ($\boldsymbol{\mu}_{MON}$, isolated molecule, white arrow; $\boldsymbol{\mu}_{MS}$, MOLSPLIT density, light gray arrow; $\boldsymbol{\mu}_{PC}$, periodic calculation, dark gray arrow). View perpendicular to the benzene ring.

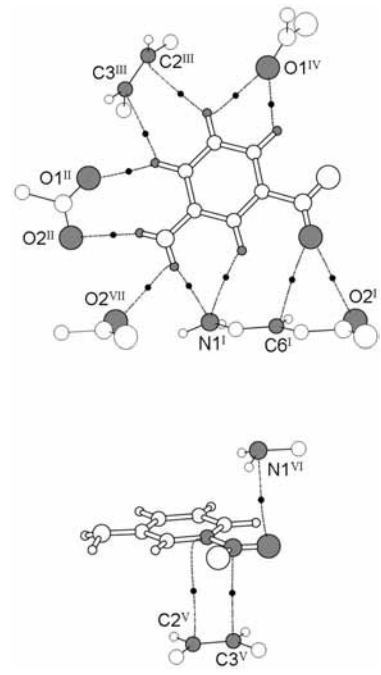

Figure 2. Intermolecular bond paths in the PC electron density of mNA; attractors are highlighted in gray, and (3, −1) critical points are drawn as black circles.

to determine the values of some electrostatic magnitudes by integration of the corresponding functions within the AIM partition atomic basins.

The XD[12] utilities were used to project the B3LYP electron densities onto the multipole model. Integration of the resulting densities in the AIM atomic basins was performed with TOPXD.[12]

Calculations involving an electric field were performed with Gaussian 03,[13] and the resulting electron densities were analyzed with the Aimpac programs.[14]

Structural data (cell parameters and atomic coordinates) were taken from ref 15 for mNA, from ref 16 for 2M5NA, from ref 17 for 2M4NA, and from ref 18 for pNA.

Results and Discussion

Topological Analysis. Within the AIM theory,[10] (3, −1) critical points corresponding to close shell interactions are characterized by a low positive value of the Laplacian of the electron density ($\nabla^2\rho_c$) and a low value of the electron density (ρ_c). For this kind of interaction, ρ_c can be used as an indicator of the interaction strength, but, when dealing with interactions that can be considered hydrogen bonds, λ_3, the positive eigenvalue of the Hessian of ρ, has proved to correlate better with the interaction energies.[19] Hence, our analyses are based on λ_3 values with regard to the relative strengths of different kinds of hydrogen bonds.

***m*-Nitroaniline.** mNA crystallizes in the space group $Pca2_1$, with one molecule in the asymmetric unit. The crystal packing has been described[20,21] in terms of polar chains generated by the lattice translations **b-c**. Adjacent chains, which are rotated 67.57(4)°, associate in the form of polar ribbons through N1−H11···N1, N1−H11···O2, and C6−H6···N1 contacts (see Figure 1a for atom labeling). These ribbons pile up building layers perpendicular to **a** centered in $x = 0.25$, where ribbons run along [01$\bar{1}$], and 0.75, where ribbons run along [0$\bar{1}$ $\bar{1}$].

TABLE 1: Topological Properties of the Intermolecular Interactions in the PC Model for mNA: Electron Density (ρ; e/Å^3), Laplacian ($\nabla^2\rho$; e/Å^5), and Positive Principal Curvature (λ_3; e/Å^5) Evaluated at the Corresponding (3, −1) Critical Points

		ρ		$\nabla^2\rho$		λ_3	
		PC	exp[a]	PC	exp[a]	PC	exp[a]
H11	$N1^{I}$	0.112	0.102 (17)	0.993	1.006 (21)	1.86	1.80
H6	$N1^{I}$	0.053	0.046 (3)	0.597	0.634 (3)	0.89	0.86
O2	$C6^{I}$	0.033	0.032 (2)	0.437	0.472 (1)	0.57	0.62
O2	$O2^{I}$	0.025	0.022 (0)	0.421	0.395 (0)	0.55	0.50
H2	$O1^{II}$	0.077	0.078 (10)	0.927	0.971 (9)	1.49	1.61
H12	$O2^{II}$	0.077	0.068 (7)	0.894	1.032 (7)	1.47	1.53
H12	$O1^{II}$		0.041 (4)		0.676 (4)		0.88
H3	$C2^{III}$	0.037	0.033 (3)	0.385	0.398 (2)	0.54	0.53
H2	$C3^{III}$	0.036	0.030 (3)	0.418	0.431 (2)	0.55	0.52
H4	$O1^{IV}$	0.048	0.042 (4)	0.653	0.649 (1)	0.95	0.90
H3	$O1^{IV}$	0.033	0.031 (3)	0.498	0.519 (1)	0.65	0.68
N2	$C3^{V}$	0.031	0.029 (1)	0.387	0.381 (1)	0.46	0.44
C5	$C2^{V}$	0.026		0.260		0.31	
C6	$C2^{V}$		0.023 (1)		0.278 (1)		0.34
O1	$N1^{VI}$	0.030	0.029 (1)	0.397	0.429 (1)	0.51	0.54
H11	$O2^{VII}$	0.034	0.032 (4)	0.530	0.530 (1)	0.71	0.66

[a] From ref 15. Symmetry codes: (I) 0.5 − *x*, *y*, 0.5 + *z*; (II) *x*, 1 + *y*, −1 + *z*; (III) −*x*, 2 − *y*, −0.5 + *z*; (IV) −*x*, 1 − *y*, −0.5 + *z*; (V) *x*, *y*, 1 + *z*; (VI) *x*, −1 + *y*, *z*; (VII) 0.5 − *x*, 1 + *y*, −0.5 + *z*.

A set of critical points satisfying the Morse relationship was characterized in the PC electron density, 14 of them being unique intermolecular (3, −1) critical points (ICP). In this way, a set of 28 bond paths link each molecule with its 14 nearest neighbors (see Figure 2). Values for the parameters characterizing the bond paths (BPs) and ICPs found in the seven unique molecular pairs are listed in Table 1, where labeling of the symmetry operations generating the pairs is also presented.

Two BPs connect neighboring molecules within a chain (symmetry operation II). One of them links the amino H12 to $O2^{II}$ and corresponds to the primary amino-nitro interaction of the crystal structure, on the basis of the classification made by

Panunto et al. in their study of H-bonding patterns in nitroaniline crystals.[22] In contrast to the three-centered nature proposed by these authors, since H12 is not bonded to $O1^{II}$ this interaction should be described as two-centered from a topological viewpoint. The other BP connects the aromatic H2 to $O1^{II}$, this interaction being the strongest of this pair.

Chains within a ribbon are linked through five BPs. Four of them connect molecules related by symmetry operation I. Two of them involve N1, so that this atom, besides being the acceptor of the $N1-H11\cdots N1^{I}$ hydrogen bond—the strongest intermolecular interaction—is connected to the aromatic hydrogen H6 through a bond path that, on geometrical and topological grounds, can be characterized as a $C-H\cdots N$ hydrogen bond. The other two BPs between molecules related by symmetry operation I are associated with $O2\cdots C6^{I}$ and $O2\cdots O2^{I}$ interactions. The remaining interaction between chains links H11 with $O2^{VII}$ and corresponds to the shortest contact of the secondary amino-nitro interaction identified in ref 22. Stacked molecules within a layer are connected through two BPs linking molecules related by symmetry operation V and one BP between the pair generated by symmetry operation VI.

Adjacent layers are connected through four BPs corresponding to two $C-H\cdots O1^{IV}$ and two $C-H\cdots C^{III}$ interactions. Based on geometry optimizations at semiempirical levels, Turi and Dannenberg[20] concluded that these $C-H\cdots O$ interactions are strong enough to be responsible for the way layers pile up in the **a** direction, giving rise to the observed polar crystal structure. The present results would support that conclusion, in that $H4\cdots O1^{IV}$ is the most relevant interlayer interaction, followed by $H3\cdots O1^{IV}$. It should be noticed, however, that the other two interlayer interactions characterized on topological grounds, $H3\cdots C2^{III}$ and $H2\cdots C3^{III}$, have λ_3 values of the same order as $H3\cdots O1^{IV}$. Bond paths associated with these $H\cdots C$ interactions are noticeably bent, particularly that linking H2 to $C3^{III}$. Indeed, its major part lies around a line through H2 and the midpoint of the $C3^{III}-C4^{III}$ bond, and only near this bond it suddenly deviates to $C3^{III}$. Though less noticeable, behavior of the $H3\cdots C2^{III}$ bond path is similar, and then both interactions can be characterized as $C-H\cdots\pi$.[23−25]

The lack of a bond path connecting H12 and O1 in the molecular pair generated by symmetry operation II is the main difference with respect to the intermolecular interactions reported in ref 15 for the experimental charge density. All the interactions identified in the PC electron density had also been found in the experimental electron density,[15] ρ_c values in the former agreeing within twice the uncertainty with their counterparts in the latter. The trend of the hydrogen bond strengths is the same in one and the other density, bond paths that significantly deviate from the interatomic line being also similar.

2-Methyl-5-nitroaniline. 2M5NA crystallizes in space group $P2_1/n$, with one molecule in the asymmetric unit. The three-dimensional structure has been described[16,26] in terms of polar chains running along $[10\bar{1}]$ and assembled head-to-tail to form nonpolar (101) layers. Connection between adjacent chains within a layer is established through a pair of molecules related by an inversion center.

Among the self-consistent set of critical points characterized in the PC electron density of 2M5NA, 15 are unique intermolecular (3, −1) critical points (ICPs). Each molecule is linked through 27 bond paths with its 13 nearest neighbors (see Figure 3). Values for the parameters characterizing the bond paths (BPs) and ICPs found in the eight unique molecular pairs are listed in Table 2, together with the labeling of the symmetry operations generating the pairs.

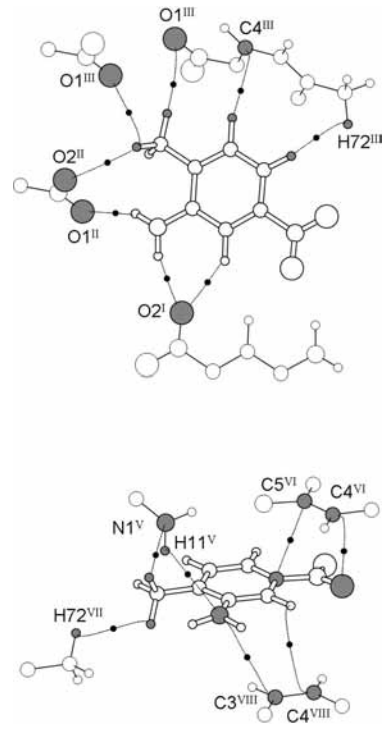

Figure 3. Intermolecular bond paths in the PC electron density of 2M5NA; attractors are highlighted in gray, and (3, −1) critical points are drawn as black circles.

TABLE 2: Topological Properties of the Intermolecular Interactions in the PC Model for 2M5NA: Electron Density (ρ; e/Å^3), Laplacian ($\nabla^2\rho$; e/Å^5), and Positive Principal Curvature (λ_3; e/Å^5) Evaluated at the Corresponding (3, −1) Critical Points

		ρ		$\nabla^2\rho$		λ_3	
		PC	exp[a]	PC	exp[a]	PC	exp[a]
H6	$O2^{I}$	0.075	0.061 (10)	0.919	0.991 (9)	1.45	1.45
H11	$O2^{I}$	0.071	0.066 (10)	0.914	0.655 (12)	1.44	1.28
H12	$O1^{II}$	0.101	0.065 (12)	1.040	1.069 (18)	1.88	1.69
H71	$O2^{II}$	0.037	0.030 (6)	0.506	0.444 (2)	0.72	0.63
H3	$C4^{III}$	0.060	0.062 (7)	0.661	0.597 (5)	0.91	0.87
H4	$H72^{III}$	0.034		0.446		0.63	
H4	$C7^{III}$		0.026 (6)		0.382 (2)		0.48
H73	$O1^{III}$	0.023	0.024 (4)	0.326	0.284 (2)	0.43	0.40
H71	$O1^{IV}$	0.038		0.558		0.72	
N1	$H11^{V}$	0.016		0.231		0.29	
H71	$N1^{V}$	0.044	0.037 (6)	0.473	0.467 (4)	0.73	0.75
C5	$C5^{VI}$	0.034		0.364		0.44	
O2	$C4^{VI}$	0.027		0.364		0.43	
H72	$H72^{VII}$	0.028		0.343		0.46	
N1	$C3^{VIII}$	0.032		0.381		0.47	
H6	$C4^{VIII}$	0.027		0.297		0.36	

[a] From ref 27. Symmetry codes: (I) $2-x, 1-y, 1-z$; (II) $x+0.5, 0.5-y, z-0.5$; (III) $1.5-x, y-0.5, 0.5-z$; (IV) $x+0.5, -0.5-y, z-0.5$; (V) $2.5-x, y-0.5, 0.5-z$; (VI) $2-x, -y, 1-z$; (VII) $-x, -y, -z$; (VIII) $x, 1+y, z$.

On the basis of its associated λ_3 value, the strongest interaction at play ($H12\cdots O1^{II}$) (see Figure 1b for atom labeling) connects the pair of molecules related through a sliding plane, giving rise to the polar chains. A much weaker $H71\cdots O2^{II}$ completes the connection along the chains. Two pairs of BPs link the centrosymmetric pair generated by I, each pair corresponding, respectively, to $H6\cdots O2^{I}$ and $H11\cdots O2^{I}$ interactions. It is interesting to note that the corresponding topological parameters of both CPs have almost identical values, in spite of the significant difference in nature between the involved H atoms.

From a topological viewpoint, the C−H···O hydrogen bond would in fact be as strong as the N−H···O one. Due to the behavior of the associated BP, the main interaction among those linking pair III can in principle be considered a C−H ···π interaction (see preceding section) involving the $C3^{III}-C4^{III}$ bond. The remaining two interactions linking this pair connect H4 with $H72^{III}$ and H73 with $O1^{III}$. The only interactions in which N1 plays the role of acceptor are found in the pair generated by symmetry operation V, the strongest involving a methyl hydrogen as donor. One C5···C5 and one pair of O2···C4 interactions link the centrosymmetric pair of stacked molecules generated by symmetry operation VI. Molecules related by symmetry operation VII are connected only through a bond path linking two equivalent methyl hydrogen atoms. Molecules in the pair generated by symmetry operation VIII are linked by two interactions, $N1-C4^{VIII}$ and $H6-C4^{VIII}$, the latter being a C−H···π having the $C3^{VIII}-C4^{VIII}$ π cloud as acceptor.

Only bond paths and topological parameters corresponding to X−H···Y intermolecular interactions were reported for the experimental charge density in ref 27. All of them were also found in the PC electron density, with the subtle difference that the H4···C7 interaction reported in ref 27 becomes a H4···H72 in the PC density. Similarly to what happens in the case of mNA, ρ_c values agree within twice the uncertainty with their counterparts in the experimental density, with the only exception of the $H12\cdots O1^{II}$ interaction. Also in this case the trend in hydrogen bond strengths and the behavior of the bond paths are similar in one and the other density. $H71\cdots O1^{IV}$ and $N1\cdots H11^{V}$ are the only X−H···Y interactions characterized in the present work for the PC electron density but absent in the experimental one.

Molecular Dipole Moment. Determination of the molecular dipole moment in a periodic system requires adopting a partition scheme to define atoms and molecules and the associated electron densities. In the partition scheme based on the AIM theory,[10] each point of real space is assigned to a particular atomic basin, so that discrete boundaries appear. In a periodic system, such boundaries correspond to surfaces of zero-flux of the $\nabla\rho$ vector field. Moments of the atomic electron densities are then determined by integration of the corresponding functions over each atomic basin. If q_i and $\boldsymbol{\mu}_i$ are the net charge and dipole moment of atom i, the molecular dipole moment can then be calculated in a straightforward manner as the summation of a monopolar ($\boldsymbol{\mu}_M$) and a dipolar ($\boldsymbol{\mu}_D$) contributions

$$\boldsymbol{\mu} = \boldsymbol{\mu}_M + \boldsymbol{\mu}_D = \sum q_i \mathbf{r}_i + \sum \boldsymbol{\mu}_i$$

Values of the atomic moments within the AIM partition scheme were obtained for the PC, MOLSPLIT, and isolated molecule (MON) densities of mNA, 2M5NA, 2M4NA, and pNA. Absolute values of the integrated $\nabla^2\rho$ are all smaller than 0.0055 au. Values of the molecular dipole moment components (in the crystal Cartesian axes system) and modulus obtained from each electron density are reported in Table 3. As can be seen, the enhancement of the molecular dipole moment modulus in going from the isolated molecule (in the crystal geometry) to the crystal amounts to 38%, 44%, 51%, and 47%, respectively, for mNA, 2M5NA, 2M4NA, and pNA.

The lack of uncertainties makes meaningless any absolute comparison between two sets of AIM dipole moment components and modulus, but agreement can always be judged in relative terms. On the other hand, comparison between values obtained directly from a periodic B3LYP density with those determined from an experimental charge density can be biased by the pseudoatom multipole model implicit in the latter. Projection of the B3LYP density onto the multipole model can be used to make both sets more directly comparable, though the equivalence between a multipole model fitted against experimental structure factors and that fitted against their theoretical counterparts can hardly be ensured.

TABLE 3: AIM Molecular Dipole Moment (D) in the Crystallographic Cartesian Axes System

	periodic calculations			molecular calculations		
	crystal	MOLSPLIT	multipole projection	uniform **E**[a]	point charges + uniform **E**	isolated molecule
			mNA			
μ_x	−0.6	−0.7	−0.5	−0.4	−0.5	−0.6
μ_y	6.8	5.7	6.1	7.1	6.9	5.0
μ_z	−4.2	−3.7	−4.8	−4.3	−4.2	−2.9
μ	8.0	6.8	7.8	8.3	8.1	5.8
			2M5NA			
μ_x	−4.9	−3.8	−4.3	−5.0	−5.0	−3.1
μ_y	−0.3	−0.1	−0.5	−0.3	−0.3	−0.4
μ_z	−7.9	−6.7	−6.8	−8.3	−8.0	−5.6
μ	9.2	7.7	8.1	9.7	9.4	6.4
			pNA			
μ_x	8.7	6.8		8.8		6.0
μ_y	−5.0	−3.9		−4.9		−3.5
μ_z	5.7	4.3		5.7		3.7
μ	11.5	9.0		11.6		7.8
			2M4NA			
μ_x	−10.3	−7.7		−10.0		−6.7
μ_y	3.3	2.4		3.3		2.3
μ_z	−5.4	−4.1		−5.3		−3.6
μ	12.1	9.1		11.8		8.0

[a] Uniform electric field components (10^{-4} au): $E_x = 0$, $E_y = 54$, $E_z = -11$ (mNA); $E_x = -44$, $E_y = -6$, $E_z = -34$ (2M5NA); $E_x = 51$, $E_y = -25$, $E_z = 52$ (pNA); $E_x = -54$, $E_y = 24$, $E_z = -33$ (2M4NA).

To test to what extent PC results are biased by the multipole model, the B3LYP periodic charge densities of mNA and 2M5NA crystals were projected onto the multipole model.[7] The same set of reciprocal vectors used in the corresponding experimental study[15] was used for mNA, while for 2M5NA all unique reflections within the range $0 < \sin(\theta/\lambda) < 1.10$ Å^{-1} were included. Refinements were performed on F, with unit weights. Atomic coordinates were fixed to the values used in the calculation. In order to mimic the effect of thermal motion on the scattering intensity as a function of angle, theoretical (static) structure factors were multiplied by $\exp[-8\pi^2 U(\sin\theta/\lambda)^2]$, with $U = 0.025$ Å^2. The global scale factor was fixed to unity. Multipolar coefficients up to octupoles were refined without constraints for non-H atoms. For H atoms, only dipolar and quadrupolar coefficients of the deformation functions with axial symmetry around the X−H bond were refined (one dipolar and one quadrupolar coefficient). One set of expansion-contraction parameters κ, κ' was assigned to each chemical species, according to the following classification: oxygen, amino nitrogen, nitro nitrogen, aromatic carbon, methyl carbon, amino hydrogen, aromatic hydrogen, and methyl hydrogen. Hydrogen κ' parameters were fixed to 1.24.

Values of the AIM molecular dipole moments obtained from the resulting electron densities for mNA and 2M5NA are reported in Table 3.

A first conclusion one can draw is that the multipole projection has little influence on the values calculated for mNA (less than 3%), but results are considerably biased in the case

of 2M5NA. AIM values corresponding to the experimental charge density are only available for mNA,[15] dipole moment modulus agreeing within 5% with the PC value, but only within 8% with the value obtained after multipole projection of the PC density.

Equivalent comparisons showed that, for 2M4NA[17] and pNA,[28] multipole projection induces changes in the AIM values of the dipole moment modulus of the same order as that reported in the present work for mNA. Agreement between theoretical and experimental values, however, is better for 2M4NA and pNA.

Molecule in the Crystal Electric Field. In an attempt to obtain information on the influence of any noninductive effect on the in-crystal molecular dipole moment enhancement, we based our analysis on model electron densities constructed as the superposition of molecular densities. This was accomplished by constructing a set of spatial orbitals (supermolecular spatial orbitals) simply as the union of sets of molecular spatial orbitals. In a first stage, individual B3LYP/6-31G** molecular calculations were performed for a reference molecule and its first neighbors in the crystal (that is all the molecules connected with the reference one by at least one bond path), and the wave function suitable to be fed in the Aimpac suite of programs (WFN) was obtained in each case. Supermolecular orbitals were then generated by assigning to each atomic center a coefficient that is either zero or equal to the corresponding coefficient in the WFN of the particular molecule to which the center belongs.

AIM atomic moments for the reference molecule were then determined. As could be expected, values of the components of the molecular dipole moment of the reference molecule obtained from them coincide with the MOLSPLIT values reported in Table 3 for any of the compounds.

The crudest approximation to account for the effects of the crystal packing on the molecular electrostatic properties is to consider the molecule acted on by a uniform electric field generated by the rest of the molecules in the crystal. As a first approximation, a mean value for the electric field a reference molecule is acted on in the crystal was estimated as follows. The electric field at the atomic positions was calculated as the difference between the corresponding values obtained from the MOLSPLIT and isolated molecule electron densities, using the algorithms in the Crystal 98 program.[29] Components of the mean electric field were then determined as the average over all the atoms in the molecule (see Table 3).

The wave function of the reference molecule in this mean electric field was then obtained, and a new superposition density was generated. Resulting AIM values of the molecular dipole moment components and modulus of the reference molecule in mNA, 2M5NA, 2M4NA, and pNA crystals are reported in Table 3. Agreement between values calculated this way with those obtained directly from the periodic calculations is better than 6%, dipole moment directions coinciding within 2°. These results can in principle be considered as an indication of the little influence of any noninductive effect with regard to the change in the molecular dipole moment in going from the isolated molecule to the crystal, in any of the four molecular systems considered in the present study.

But what deserves additional consideration is the good performance of the apparently rough uniform electric field approximation. To further test its validity, for mNA and 2M5NA the procedure described above was carried through again, this time employing a nonuniform electric field. This field was defined as the superposition of the field generated by a set of point charges located at the atomic positions of the neighboring molecules in the cluster and a new uniform field. Point charges were obtained from a fit to the electrostatic potential of the isolated molecule within the MKS scheme.[30] The new uniform electric field, which approximates the influence of all the molecules in the crystal other than first neighbors, was determined by subtracting from the uniform field used in the above-described calculations the average over all the central molecule atom positions of the field generated by the point charges. This way, the uniformity of the electric field the central molecule is acted on is lifted, but its mean value is the same as before. The resulting central molecule WFN was then used in the procedure already described. With respect to the preceding case, agreement of the resulting AIM dipole moment components with their PC counterparts is improved, but what is remarkable is that changes are smaller than 4% (see Table 3).

It is worth noting that a uniform field approximation had already been used by Spackman et al.[31] to study the enhancement of the molecular dipole moment in a wide range of molecular crystals. Though comparison is not necessarily straightforward, with regard to the four systems analyzed in the present work there is in general good agreement between the results reported in that paper with those in Table 3. In particular, the intensity of the uniform fields used here compare well with the F_0 values of ref 31. Keeping in mind that also the values reported in Table 3 imply approximations, that fact makes evident the good performance of the dipole lattice sum method used in that case. In comparing dipole moment moduli, two main factors must be taken into account. On the one hand, our results for the molecule in the presence of an electric field should in principle be compared with the μ_1 values of ref 31, and, on the other hand, they refer to a molecule with discrete boundaries, as that implicit in the periodic calculations. Assuming the effect of this partition difference is independent of the applied electric field, it could be associated with the difference between the MS and isolated molecule dipole moments, its value being about 1.2 D for the four systems considered in the present study.

Conclusions

A set of intermolecular bond paths in reasonable agreement with its experimental counterpart was characterized in the B3LYP/6-31G** electron density of mNA and 2M5NA crystals, this fact revealing that, in spite of its limitations with regard to the electron correlation treatment, the B3LYP hybrid method leads to a reasonable description of the rather low intermolecular electron density, at least as concerns the nature and relative importance of the intermolecular interactions at play.

The superposition of molecular electron densities in real space was used to build a model charge density for a reference molecule surrounded by its nearest neighbors in the crystal. This method, which relies only on single-molecule calculations, allows the definition of a molecule with a finite zero-flux boundary whose properties can be directly compared to those resulting from a periodic calculation.

For the four crystals included in the present study, the in-crystal molecule dipole moment obtained from a periodic calculation at the B3LYP/6-31G** level was found to be reproducible within 6% by a superposition density of that kind, if the density of the reference molecule acted on by a uniform electric field is used. This finding can be taken as an indication that the molecular dipole moment enhancement in these systems is due solely to inductive effects. Moreover, results are almost unchanged if the nonuniformity of the crystal field is taken into account by means of a distribution of point charges, a fact that reflects that the main mechanism of dipole moment enhancement is the overall intramolecular charge transfer.

Acknowledgment. The authors are grateful to CONICET, UNLP, and ANPCyT (PICT 2315), for financial help. A.F. and G.P. are members of CONICET. C.G.P. acknowledges a CONICET fellowship.

References and Notes

(1) Bosshard, Ch.; Hulliger, J.; Florsheimer, M.; Gunter, P. *Organic Nonlinear Optical Materials*; Advances in Nonlinear Optics Vol. 1; Gordon and Breach Science Publishers SA: Amsterdam, 1995.

(2) Cole, J. M. *Philos. Trans. R. Soc. London, Ser. A* **2003**, *361*, 2751.

(3) Marder, S. R. *Chem. Commun.* **2006**, 131.

(4) Ros, M. B. *Organic Materials for Nonlinear Optics in Engineering of Crystalline Materials Properties. State of the Art in Modeling, Design and Applications*; Novoa, J., Braga, D., Addadi, L., Eds.; Springer: The Netherlands, 2008.

(5) Koos, C.; Vorreau, P.; Vallaitis, T.; Dumon, P.; Bogaerts, W.; Baets, R.; Esembeson, B.; Biaggio, I.; Michinobu, T.; Diederich, F.; Freude, W.; Leuthold, J. *Nat. Photonics* **2009**, *3*, 216.

(6) Hecht, J. *Laser Focus World Magazine* **2008**, *44*, 1, and references therein.

(7) Hansen, N. K.; Coppens, P. *Acta Crystallogr.* **1978**, *A34*, 909.

(8) Spackman, M. A.; Munshi, P.; Dittrich, B. *Chem. Phys. Chem.* **2007**, *8*, 2051.

(9) Saunders, V. R.; Dovesi, R.; Roetti, C.; Causà, M.; Harrison, N. M.; Orlando, R.; Zicovich-Wilson, C. M. *CRYSTAL98 User's Manual*; University of Torino: Torino, Italy, 1998.

(10) (a) Bader, R. F. W. *Atoms in Molecules: A Quantum Theory*; Clarendon Press, Oxford Science Publications: Oxford, 1990. (b) Popelier, P. *Atoms in Molecules: An Introduction*; Prentice Hall: Harlow, 2000. (c) *The Quantum Theory of Atoms in Molecules: From Solid State to DNA and Drug Design*; Matta, C. F., Boyd, R. J., Eds.; Wiley-VCH: Weinheim, 2007.

(11) Gatti, C. *TOPOND 98 User's Manual*; CNR-ISTM: Milano, 1999.

(12) Volkov, A.; Macchi, P.; Farrugia, L. J.; Gatti, C.; Mallinson, P.; Richter, T.; Koritsanszky, T. *XD2006—A computer program package for multipole refinement, topological analysis of charge densities and evaluation of intermolecular energies from experimental and theoretical structure factors*, 2006.

(13) Frisch, M. J.; Trucks, G. W.; Schlegel, H. B.; Scuseria, G. E.; Robb, M. A.; Cheeseman, J. R.; Montgomery, J. A., Jr.; Vreven, T.; Kudin, K. N.; Burant, J. C.; Millam, J. M.; Iyengar, S. S.; Tomasi, J.; Barone, V.; Mennucci, B.; Cossi, M.; Scalmani, G.; Rega, N.; Petersson, G. A.; Nakatsuji, H.; Hada, M.; Ehara, M.; Toyota, K.; Fukuda, R.; Hasegawa, J.; Ishida, M.; Nakajima, T.; Honda, Y.; Kitao, O.; Nakai, H.; Klene, M.; Li, X.; Knox, J. E.; Hratchian, H. P.; Cross, J. B.; Bakken, V.; Adamo, C.; Jaramillo, J.; Gomperts, R.; Stratmann, R. E.; Yazyev, O.; Austin, A. J.; Cammi, R.; Pomelli, C.; Ochterski, J. W.; Ayala, P. Y.; Morokuma, K.; Voth, G. A.; Salvador, P.; Dannenberg, J. J.; Zakrzewski, V. G.; Dapprich, S.; Daniels, A. D.; Strain, M. C.; Farkas, O.; Malick, D. K.; Rabuck, A. D.; Raghavachari, K.; Foresman, J. B.; Ortiz, J. V.; Cui, Q.; Baboul, A. G.; Clifford, S.; Cioslowski, J.; Stefanov, B. B.; Liu, G.; Liashenko, A.; Piskorz, P.; Komaromi, I.; Martin, R. L.; Fox, D. J.; Keith, T.; Al-Laham, M. A.; Peng, C. Y.; Nanayakkara, A.; Challacombe, M.; Gill, P. M. W.; Johnson, B.; Chen, W.; Wong, M. W.; Gonzalez, C.; Pople, J. A. *Gaussian 03*, revision D.01; Gaussian, Inc.: Wallingford, CT2004.

(14) Biegler-König, F.; Bader, R. F. W.; Tang, W. H. *J. Comput. Chem.* **1982**, *3*, 317.

(15) Pozzi, C. G.; Fantoni, A. C.; Punte, G.; Goeta, A. E. *Chem. Phys.* **2009**, *358*, 68.

(16) Ellena, J.; Goeta, A. E.; Howard, J. A. K.; Wilson, C. C.; Autino, J. C.; Punte, G. *Acta Crystallogr.* **1999**, *B55*, 209.

(17) Whitten, A. E.; Turner, P.; Klooster, W. T.; Piltz, R. O.; Spackman, M. A. *J. Phys. Chem. A* **2006**, *110*, 8763.

(18) Pozzi, C. G.; Goeta, A. E.; Punte, G.; de Matos Gomes, E.; Belsley, M.; McIntyre, G. J. *Acta Crystallogr., Sect. A Suppl.* **2005**, *61*, C394.

(19) Espinosa, E.; Souhassou, M.; Lachekar, H.; Lecomte, C. *Acta Crystallogr.* **1999**, *B55*, 563.

(20) Turi, L.; Dannenberg, J. J. *J. Phys. Chem.* **1996**, *100*, 9638.

(21) Goeta, A. E.; Wilson, C. C.; Autino, J. C.; Ellena, J. A.; Punte, G. *Chem. Mater.* **2000**, *12*, 3342.

(22) Panunto, T. W.; Urbánczyk-Lipkowska, Z.; Johnson, R.; Etter, M. C. *J. Am. Chem. Soc.* **1987**, *109*, 7786.

(23) Rozas, I.; Alkorta, I.; Elguero, J. *J. Phys. Chem. A* **1997**, *101*, 9457.

(24) Tang, T. H.; Cui, Y. P. *Can. J. Chem.* **1996**, *74*, 1162.

(25) Novoa, J. J.; Mota, F. *Chem. Phys. Lett.* **2000**, *318*, 345.

(26) Ellena, J.; Punte, G.; Rivero, B. E. *J. Chem. Crystallogr.* **1996**, *26*, 319.

(27) Ellena, J. A.; Goeta, A. E.; Howard, J. A. K.; Punte, G. *J. Phys. Chem. A* **2001**, *105*, 8696.

(28) Volkov, A.; Gatti, C.; Abramov, Y.; Coppens, P. *Acta Crystallogr.* **2000**, *A56*, 252.

(29) Saunders, V. R.; Freyria-Fava, C.; Dovesi, R.; Salasco, L.; Roetti, C. *Mol. Phys.* **1992**, *77*, 629.

(30) Singh, U. C.; Kollman, P. A. *J. Comput. Chem.* **1984**, *5*, 129.

(31) Spackman, M. A.; Munshi, P.; Jayatilaka, D. *Chem. Phys. Lett.* **2007**, *443*, 87.

JP904318Q